energies

MDPI

Article

Sliding Mode Control of a Variable- Speed Wind Energy Conversion System Using a Squirrel Cage Induction Generator

Mohamed Zribi, Muthana Alrifai * and Mohamed Rayan

Department of Electrical Engineering, Kuwait University, P. O. Box 5969, Safat 13060, Kuwait; mohamed.zribi@ku.edu.kw (M.Z.); m.rayan@ku.edu.kw (M.R.)
* Correspondence: m.alrifai@ku.edu.kw; Tel.: +965-2498-7381

Academic Editor: Frede Blaabjerg
Received: 25 January 2017; Accepted: 19 April 2017; Published: 1 May 2017

Abstract: This paper deals with the control of a variable-speed wind energy conversion (WEC) system using a squirrel cage induction generator (SCIG) connected to the grid through a back-to-back three phase (AC-DC-AC) power converter. The sliding mode control technique is used to control the WEC system. The objective of the controllers is to force the states of the system to track their desired states. One controller is used to regulate the generator speed and the flux so that maximum power is extracted from the wind. Another controller is used to control the grid side converter, which controls the DC bus voltage and the active and reactive powers injected into the grid. The performance of the controlled wind energy conversion system is verified through MATLAB simulations, which show that the controlled system performs well.

Keywords: wind energy conversion; squirrel cage induction generator (SCIG); sliding mode control

1. Introduction

Wind energy has been used to generate electricity for a long time. However, it is more prevalent nowadays because the cost of wind energy has continuously dropped, and it is approaching the competitive level of conventional energy [1]. Moreover, wind energy generation does not contribute to the pollution of the environment. The generators that are used to convert the mechanical power obtained from the wind turbine into electric power are generally either doubly-fed induction generators (DFIG), or squirrel cage induction generators (SCIG), or permanent magnet synchronous generators (PMSG). Therefore, variable-speed wind energy conversion systems can be broadly classified into three types: (i) DFIG-based wind energy conversion (WEC) systems; (ii) SCIG-based WEC systems; and (iii) PMSG-based WEC systems. For variable-speed operations, all three above-mentioned WEC systems need power electronic converters. The PMSG- and the SCIG-based systems need full-scale power electronic converters, whereas the DFIG-based systems need partial-scale power converters. Compared to the DFIG-based systems, the PMSG- and the SCIG-based systems could be more attractive due to the dropping cost of power electronics over time and due to the absence of brushes [2]. Hence, the main advantages of SCIG-based systems are their reliability, their ruggedness in design and their low operation and maintenance costs.

In an SCIG-based WEC system, the generator is coupled to the grid through back-to-back three-phase (AC-DC-AC) power converters. The AC/DC converter or the stator side converter controls the generator; the DC/AC converter or the grid side converter controls the DC bus voltage and the active and reactive powers injected into the grid. The controllers are designed so that maximum power is extracted from the wind at all wind speeds; thus, maximum system efficiency is achieved; the generated active power is transmitted through the DC-bus to the grid while ensuring the unity power factor. This paper proposes the use of the sliding mode control technique to control both the stator side and the grid side converters of an SCIG-based wind energy conversion system.

Extensive work was done on wind energy conversion systems. Mahela and Shaik [3] presented an overview of wind energy generation systems. Cheng and Zhu [4] surveyed the state of the art of wind energy conversion systems and their technologies. Chen et al. [5] reviewed the power electronics used for wind turbines systems. Papers by [1,6–8] discussed the state of the art of the control techniques applied to the different types of wind energy conversion systems.

Several control techniques were used to control the SCIG-based wind energy conversion system. Benchagra and his colleagues [9–13] published several papers on the control of SCIG-based WEC systems. Wang et al. [14] proposed a passivity-based robust controller for an SCIG-based WEC system. Hassan [15] used the backstepping control technique to control an SCIG-based WEC system. Zhao et al. [16] used an adaptive controller for maximum power point tracking (MPPT) for an SCIG-based WEC system. Heydari-doostabad et al. [17] proposed an optimal linear quadratic regulator (LQR) controller for a SCIG-based WEC system using a static compensator (STATCOM). Baloch et al. [18] employed the feedback linearization technique through field control concepts to control an SCIG-based WEC system. Domínguez-García [19] used indirect vector control for the squirrel cage induction generator WEC system. The sliding mode control (SMC) technique was used for induction generator-based WEC systems in [20–24]. Moreover, other types of controllers were also designed for squirrel cage-based WEC systems; for example, see [25–31].

The sliding mode technique is a very suitable approach to deal with the control of wind energy conversion systems. This is the case because this technique is robust with respect to variations in the parameters of the system and to bounded external disturbances. Therefore, the SMC technique is selected to control the squirrel cage induction generator-based WEC system.

The contribution of this paper involves the design of two controllers, which force the states of a squirrel cage induction generator-based wind energy conversion system to track the desired states of the system and the transmission of the the generated power to the grid. The first sliding mode controller enables maximum extraction of power from the wind at different speeds of the wind; the second sliding mode controller ensures that the generated active power is injected through the DC-bus to the grid with the unity power factor. The proposed controllers are validated through MATLAB simulation.

The rest of the paper is organized as follows. The model of an SCIG-based wind energy conversion system is presented in Section 2. The model of the system consists of two parts. The first part is composed of the model of the wind turbine and the induction generator; the second part consists of the model of the grid side converter. The computation of the desired states of the WEC system and the computation of the reference inputs are presented in Section 3. The design of sliding mode controllers for the WEC system is proposed in Section 4. Simulation results for the controlled system are presented and discussed in Section 5. Finally, the conclusion is given in Section 6.

2. Model of the Wind Energy Conversion System

This section presents the model of the wind energy conversion system, which is depicted in Figure 1. The model of the system consists of two parts. One part deals with the model of the turbine and the squirrel cage induction generator (SCIG). This part of the system will be controlled through the stator side AC/DC Converter. The second part of the model deals with the grid side DC/AC converter sub-system.

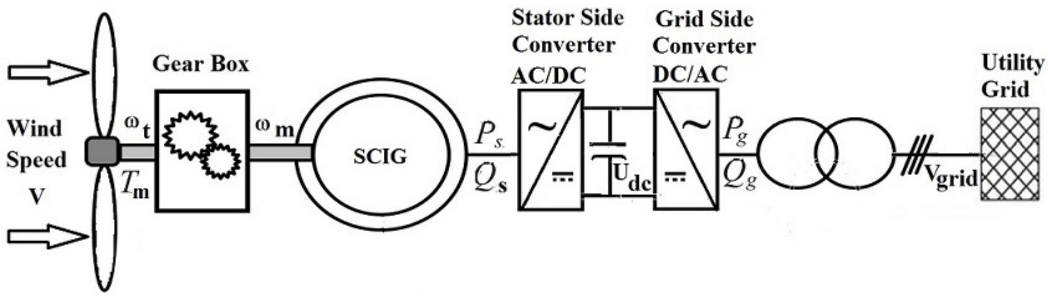

Figure 1. A block diagram representation of the squirrel cage induction generator (SCIG)-based wind energy conversion (WEC) system.

2.1. The Model of the Turbine and the Induction Generator

The mechanical power extracted from the wind can be expressed as follows:

$$P_m = \frac{1}{2}C_p(\lambda,\beta)\rho A V^3 \quad (1)$$

where P_m is the mechanical output power of the wind turbine; the power coefficient is represented by $C_p(\lambda,\beta)$; λ is the tip speed ratio (TSR) of the turbine blade; and β is the pitch angle. The constant ρ represents the air density; A is the area swept by the rotor blades; and V is the speed of the wind.

The gearbox transfers power from the rotating wind turbine shaft to the rotating generator shaft. The angular speed of the generator ω_m is related to the angular speed of the wind turbine ω_t through the following equation:

$$\omega_m = G\,\omega_t \quad (2)$$

where G is the gear ratio.

The tip speed ratio is related to the angular speed of the wind turbine ω_t and the angular speed of the generator ω_m through the following equation:

$$\lambda = \frac{R\omega_t}{V} = \frac{R\omega_m}{GV} \quad (3)$$

where R is the radius of the turbine blades.

The power coefficient C_p is a nonlinear function of λ; several nonlinear models of C_p can be found in the literature. The model of the power coefficient adopted in this paper is as follows [32]:

$$C_p(\lambda,\beta) = a_1\left(\frac{a_2}{\bar{\lambda}} - a_3\beta - a_4\right)exp\left(-\frac{a_5}{\bar{\lambda}}\right) + a_6\lambda \quad (4)$$

where $\bar{\lambda} = 1/[1/(\lambda + a_7\beta) - a_8/(\beta^3+1)]$ with $a_1 = 0.5109$, $a_2 = 116$, $a_3 = 0.4$, $a_4 = 5$, $a_5 = 21$, $a_6 = 0.0068$, $a_7 = 0.08$ and $a_8 = 0.035$. Figure 2 depicts the power coefficient C_p versus the tip speed ratio λ for different pitch angles. The figure shows that the maximum value of the power coefficient C_p is $C_{p_{max}} = 0.47$; this value is obtained when the pitch angle β equals zero degrees and the corresponding optimum tip speed ratio is $\lambda_{opt} = 8.1$.

Note that the maximum mechanical power extracted from the wind is such that:

$$P_{m_{max}} = \frac{1}{2}C_{p_{max}}\lambda_{opt}\rho A V^3 \quad (5)$$

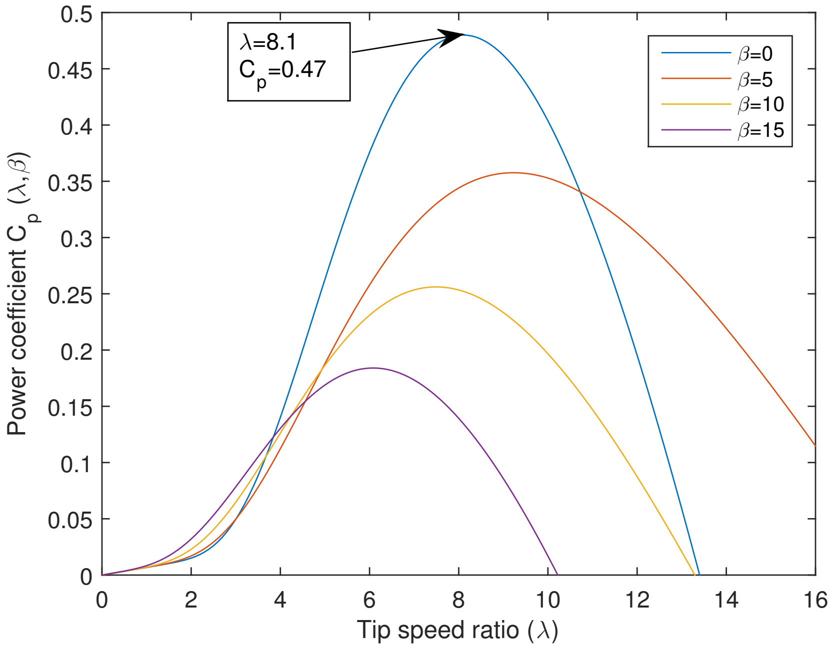

Figure 2. The power coefficient C_p versus the tip speed ratio λ for several values of the pitch angle β.

Figure 3 shows the wind turbine mechanical (aerodynamic) power P_m versus the generator speed ω_m for different values of the wind velocity V. Furthermore, the graph of the maximum mechanical power $P_{m_{max}}$ is shown in black in Figure 3.

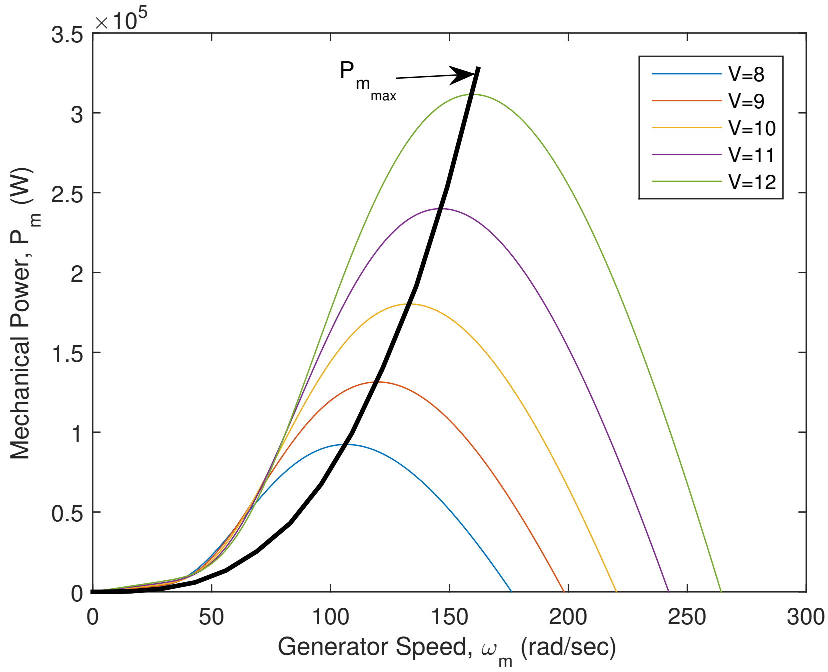

Figure 3. The mechanical power P_m versus the generator speed ω_m for several values of the wind speed V.

The mechanical (or aerodynamic) torque is related to the the power P_m captured by the wind turbine through the equation:

$$T_m = \frac{P_m}{\omega_t} \tag{6}$$

The mechanical equation of the system is such that:

$$J\frac{d\omega_m}{dt} = T_{em} - T_m - B\omega_m \tag{7}$$

In the above equation, T_{em} is the electromagnetic torque of the induction generator, and the inertia J is the total inertia of the turbine and the induction generator. This inertia is calculated such that $J = \frac{J_t}{G^2} + J_g$ where J_t and J_g represent the inertia of the turbine and the inertia of the generator respectively, and G is the gearbox ratio. Furthermore, B is the total external damping of the system.

In the direct-quadrature frame, the differential equations governing the flux linkages of the stator and the rotor of the generator are as follows [9]:

$$\frac{d\psi_{ds}}{dt} = -R_s i_{ds} + \omega_s \psi_{qs} + v_{ds} \tag{8}$$

$$\frac{d\psi_{qs}}{dt} = -R_s i_{qs} - \omega_s \psi_{ds} + v_{qs} \tag{9}$$

$$\frac{d\psi_{dr}}{dt} = -R_r i_{dr} + \omega_r \psi_{qr} \tag{10}$$

$$\frac{d\psi_{qr}}{dt} = -R_r i_{qr} - \omega_r \psi_{dr} \tag{11}$$

where ψ_{ds} is the stator direct axis flux linkage and ψ_{qs} is the stator quadrature axis flux linkage. The flux ψ_{dr} is the rotor direct axis flux linkage, and ψ_{qr} is the rotor quadrature axis flux linkage. The currents i_{ds} and i_{qs} are the stator currents in the direct-quadrature frame; and i_{dr} and i_{qr} are the rotor currents in the direct-quadrature frame. The voltages v_{ds} and v_{qs} represent the voltages of the windings of the stator in the direct-quadrature frame. The resistances R_s and R_r are the stator and rotor phase resistances. Furthermore, ω_s is the synchronous speed, and ω_r is the angular speed of the rotor.

The relationship between the stator and rotor flux linkages and the currents can be expressed as:

$$\psi_{ds} = L_s i_{ds} + L_m i_{dr} \tag{12}$$

$$\psi_{qs} = L_s i_{qs} + L_m i_{qr} \tag{13}$$

$$\psi_{dr} = L_r i_{dr} + L_m i_{ds} \tag{14}$$

$$\psi_{qr} = L_r i_{qr} + L_m i_{qs} \tag{15}$$

where L_s is the stator inductance and L_r is the rotor inductance; L_m is the mutual inductance between the stator and the rotor.

The equation of the electromagnetic torque T_{em} in the d-q frame can be written as follows:

$$T_{em} = \frac{pL_m}{L_r}(\psi_{dr} i_{qs} - \psi_{qr} i_{ds}) \tag{16}$$

where p is the number of pole pairs.

The active and reactive powers transmitted by the stator P_s and Q_s can be expressed as:

$$P_s = \frac{3}{2}(v_{ds} i_{ds} + v_{qs} i_{qs}) \tag{17}$$

$$Q_s = \frac{3}{2}(v_{ds} i_{qs} - v_{qs} i_{ds}) \tag{18}$$

Combining Equations (7)–(16), we can write the following system of ordinary differential equations (o.d.e.'s):

$$\begin{aligned}
\frac{di_{ds}}{dt} &= -c_1 i_{ds} + \omega_s i_{qs} + c_2\psi_{dr} + c_3\omega_m\psi_{qr} + c_4 v_{ds} \\
\frac{di_{qs}}{dt} &= -c_1 i_{qs} - \omega_s i_{ds} + c_2\psi_{qr} - c_3\omega_m\psi_{dr} + c_4 v_{qs} \\
\frac{d\psi_{dr}}{dt} &= c_5 i_{ds} - c_6\psi_{dr} + (\omega_s - p\omega_m)\psi_{qr} \\
\frac{d\psi_{qr}}{dt} &= c_5 i_{qs} - c_6\psi_{qr} - (\omega_s - p\omega_m)\psi_{dr} \\
\frac{d\omega_m}{dt} &= c_7(\psi_{dr} i_{qs} - \psi_{qr} i_{ds}) - c_8\omega_m - c_9 T_m
\end{aligned} \tag{19}$$

where, $c_1 = \frac{L_r^2 R_s + L_m^2 R_r}{\sigma L_s L_r^2}$, $c_2 = \frac{L_m R_r}{\sigma L_s L_r^2}$, $c_3 = \frac{pR_r}{\sigma L_s L_r}$, $c_4 = \frac{1}{\sigma L_s}$, $c_5 = \frac{L_m R_r}{L_r}$, $c_6 = \frac{R_r}{L_r}$, $c_7 = \frac{pL_m}{JL_r}$, $c_8 = \frac{B}{J}$, $c_9 = \frac{1}{J}$.

By fixing the direct axis of the rotating d-q reference frame on the rotating flux vector, we obtain $\psi_{qr} = 0$. Therefore, the corresponding equation is removed from the model of the system, and the system of o.d.e's is reduced accordingly. Furthermore, we will define the state variable vector x_T comprised of the states x_1–x_4, such that:

$$x_T = [x_1 \;\; x_2 \;\; x_3 \;\; x_4]^T = [i_{ds} \;\; i_{qs} \;\; \psi_{dr} \;\; \omega_m]^T \tag{20}$$

Therefore, the model of the wind turbine and the induction generator in (20) can be written in compact form as follows:

$$\begin{aligned}
\dot{x}_1 &= -c_1 x_1 + \omega_s x_2 + c_2 x_3 + c_4 v_{ds} \\
\dot{x}_2 &= -c_1 x_2 - \omega_s x_1 - c_3 x_3 x_4 + c_4 v_{qs} \\
\dot{x}_3 &= c_5 x_1 - c_6 x_3 \\
\dot{x}_4 &= c_7 x_2 x_3 - c_8 x_4 - c_9 T_m
\end{aligned} \tag{21}$$

We will define the desired state vector x_d such that, $x_d = [x_{1d} \;\; x_{2d} \;\; x_{3d} \;\; x_{4d}]^T = [i^*_{ds} \;\; i^*_{qs} \;\; \psi^*_{dr} \;\; \omega^*_m]^T$ where x_{id} $(i = 1, 2, ..., 4)$ are the desired values of the states x_i $(i = 1, 2, ..., 4)$ of the WEC system in (21). Since the desired states have to be an operating point of the WEC system, then these states must satisfy the model of the WEC system in (21). Therefore, the desired states of the model of the wind turbine and the induction generator system are governed by the following set of differential equations:

$$\dot{x}_{1d} = -c_1 x_{1d} + \omega_s x_{2d} + c_2 x_{3d} + c_4 v_{ds_r} \tag{22}$$

$$\dot{x}_{2d} = -c_1 x_{2d} - \omega_s x_{1d} - c_3 x_{3d} x_{4d} + c_4 v_{qs_r} \tag{23}$$

$$\dot{x}_{3d} = c_5 x_{1d} - c_6 x_{3d} \tag{24}$$

$$\dot{x}_{4d} = c_7 x_{2d} x_{3d} - c_8 x_{4d} - c_9 T_{mr} \tag{25}$$

Note that v_{ds_r}, v_{qs_r} and T_{mr} in (22), (23) and (25) are the reference input voltages and the reference mechanical torque of the WEC system. The computation of desired states and the reference inputs will be discussed in Section 3.

Define the errors e_i $(i = 1, 2, ..., 4)$ such that:

$$e_i = x_i - x_{id} \tag{26}$$

Using Equations (21)–(26), the dynamic model of the error of the wind turbine and the induction generator system can be written such that:

$$\begin{aligned} \dot{e}_1 &= -c_1e_1 + \omega_s e_2 + c_2 e_3 + c_4 u_1 \\ \dot{e}_2 &= -c_1 e_2 - \omega_s e_1 - c_3(e_3 e_4 + x_{4d} e_3 + x_{3d} e_4) + c_4 u_2 \\ \dot{e}_3 &= c_5 e_1 - c_6 e_3 \\ \dot{e}_4 &= c_7(e_2 e_3 + x_{3d} e_2 + x_{2d} e_3) - c_8 e_4 - c_9(T_m - T_{mr}) \end{aligned} \quad (27)$$

where the inputs u_1 and u_2 are defined such that:

$$u_1 = v_{ds} - v_{ds_r} \quad (28)$$

$$u_2 = v_{qs} - v_{qs_r} \quad (29)$$

In Section 4, we will use the sliding mode control technique to design the controllers u_1 and u_2 to force the errors e_1–e_4 to converge to zero as t tends to infinity.

2.2. The Model of the Grid Side Converter

The following equations relate the grid, converter voltages and the line currents [10]:

$$\begin{aligned} v_{g_1} &= R_t i_{g_1} + L_t \frac{di_{g_1}}{dt} + v_{i_1} \\ v_{g_2} &= R_t i_{g_2} + L_t \frac{di_{g_2}}{dt} + v_{i_2} \\ v_{g_3} &= R_t i_{g_3} + L_t \frac{di_{g_3}}{dt} + v_{i_3} \end{aligned} \quad (30)$$

where, v_{g_1}, v_{g_2} and v_{g_3} are the three phase grid voltages; and i_{g_1}, i_{g_2} and i_{g_3} are the line currents. The voltages, v_{i_1}, v_{i_2} and v_{i_3} are the voltages of the voltage source inverter (VSI). The resistance and the inductance of the grid-side transmission line are R_t and L_t, respectively.

Using the d-q transformation, the equations in (31) can be written as:

$$\begin{aligned} v_{dg} &= v_{d_i} - R_t i_{dg} - L_t \tfrac{di_{dg}}{dt} + \omega L_t i_{qg} \\ v_{qg} &= v_{q_i} - R_t i_{qg} - L_t \tfrac{di_{qg}}{dt} - \omega L_t i_{dg} \end{aligned} \quad (31)$$

where v_{dg} is the direct component of the grid voltage, and v_{qg} is the quadrature component of the grid voltage. The currents i_{dg} and i_{qg} are the direct and quadrature output line currents. The voltages v_{d_i} and v_{q_i} are the direct and quadrature VSI input voltages. Furthermore, $\omega = 2\pi f$, where f is the frequency of the grid.

Let the constants c_{10} and c_{11} be such that $c_{10} = \frac{R_t}{L_t}$ and $c_{11} = \frac{1}{L_t}$. Therefore, the above equations can be written as:

$$\begin{aligned} \tfrac{di_{dg}}{dt} &= -c_{10} i_{dg} + \omega i_{qg} + c_{11}(v_{d_i} - v_{dg}) \\ \tfrac{di_{qg}}{dt} &= -c_{10} i_{qg} - \omega i_{dg} + c_{11} v_{q_i} \end{aligned} \quad (32)$$

The output active power P_g and the output reactive power Q_g of the wind energy conversion system can be written as:

$$\begin{aligned} P_g &= \tfrac{3}{2}(v_{dg} i_{dg} + v_{qg} i_{qg}) \\ Q_g &= \tfrac{3}{2}(v_{qg} i_{dg} - v_{dg} i_{qg}) \end{aligned} \quad (33)$$

Setting the initial angle of the direct and quadrature reference frame to $\frac{\pi}{2}$ and setting the initial angle of Phase 1 to 0^o yield the voltage $v_{qg} = 0$ and $v_{dg} = V_{grid}$, where V_{grid} is the grid voltage. Hence, the output active and reactive powers of the system can be written as:

$$P_g = \frac{3}{2} v_{dg} i_{dg} \tag{34}$$

$$Q_g = -\frac{3}{2} v_{dg} i_{qg} \tag{35}$$

The voltage equation for the DC-bus is such that:

$$C\frac{dU_{dc}}{dt} = i_{dc} = i_s - i_g \tag{36}$$

where U_{dc} is the voltage of the DC-link, i_s is the current from the induction generator side and i_g is the current from the grid side; refer to Figure 4. The capacitor of the DC-link is denoted as C.

Remark 1. *The DC-bus voltage and the output active and reactive powers P_g and Q_g of the wind energy conversion system are controlled by the direct and quadrature components of the line current i_g. Hence, the term i_s in Equation (36) can be assumed as a disturbance in the control [15].*

Motivated by the work in [9], we multiply both sides of (36) by U_{dc} and use the fact that the SCIG active power can be expressed as $P_s = U_{dc} i_s$ and that $P_g = U_{dc} i_g$, to obtain the following equation:

$$\frac{1}{2} C \frac{dU_{dc}^2}{dt} = P_s - P_g \tag{37}$$

Using the expression $P_g = \frac{3}{2} v_{dg} i_{dg}$, the above equation can be written as:

$$\frac{dU_{dc}^2}{dt} = -\frac{3}{C} v_{dg} i_{dg} + \frac{2}{C} P_s \tag{38}$$

We will define the state variable vector x_C, which contains the states of the converter x_5–x_7, such that:

$$x_C = [x_5 \;\; x_6 \;\; x_7]^T = [i_{dg} \;\; i_{qg} \;\; U_{dc}^2]^T \tag{39}$$

Using Equations (32) and (38), the dynamic model of the grid side converter can be written as follows:

$$\begin{aligned} \dot{x}_5 &= -c_{10} x_5 + \omega x_6 + c_{11}(v_{d_i} - v_{dg}) \\ \dot{x}_6 &= -c_{10} x_6 - \omega x_5 + c_{11} v_{q_i} \\ \dot{x}_7 &= -\frac{3}{C} x_5 v_{dg} + \frac{2}{C} P_s \end{aligned} \tag{40}$$

Let $x_{5d} = i_{dg}^*$, $x_{6d} = i_{qg}^*$ and $x_{7d} = U_{dc}^{2\,*}$ represent the desired values of i_{dg}, i_{qg} and U_{dc}^2 respectively. Furthermore, let c_{12} be such that $c_{12} = \frac{3}{C}$. Define the errors e_5, e_6 and e_7 such that:

$$e_i = x_i - x_{id} \quad (i = 5,\ 6,\ 7) \tag{41}$$

The model of the errors of the grid side converter can be written as:

$$\begin{aligned} \dot{e}_5 &= -c_{10}e_5 + \omega e_6 + u_3 \\ \dot{e}_6 &= -c_{10}e_6 - \omega e_5 + u_4 \\ \dot{e}_7 &= -c_{12}e_5 v_{dg} + d_p \end{aligned} \tag{42}$$

where:

$$u_3 = -c_{10}x_{5d} + \omega x_{6d} - \dot{x}_{5d} + c_{11}(v_{d_i} - v_{dg}) \tag{43}$$

$$u_4 = -c_{10}x_{6d} - \omega x_{5d} - \dot{x}_{6d} + c_{11}v_{q_i} \tag{44}$$

$$d_p = -c_{12}x_{5d}v_{dg} - \dot{x}_{7d} + \frac{2}{C}P_s \tag{45}$$

The objective of controlling the grid side converter is to design the controllers u_3 and u_4 so that the errors e_5, e_6 and e_7 converge to zero even with the existence of the bounded "disturbance" d_p. We will use the sliding mode control technique to accomplish this task.

3. Computation of the Desired States and the Reference Inputs of the System

This section deals with the computation of the desired states and the reference inputs of the wind energy conversion system. Assuming the d-axis of the rotating frame is aligned with the rotor flux vector, then the quadrature component of the flux of the rotor is equal to zero ($\psi_{qr} = 0$), and the direct component of the flux of the rotor is always at a maximum constant value. Therefore, we can write the following:

$$x_{3d} = \psi^*_{dr} = \psi_{r_{max}} \tag{46}$$

where ψ^*_{dr} is the desired value of ψ_{dr}, and:

$$\psi_{r_{max}} = L_m i_{ds} \tag{47}$$

Furthermore, the desired value of the current i_{ds} can be calculated from (47), such that:

$$x_{1d} = i^*_{ds} = \frac{1}{L_m}\psi^*_{dr} = \frac{1}{L_m}x_{3d} \tag{48}$$

The wind turbine changes its speed by following the maximum of the power coefficient $C_{p_{max}}$, so that maximum power is extracted from the wind. Using Equation (3), the desired value of the rotor speed ω_m is such that:

$$x_{4d} = \omega^*_m = \frac{G\lambda_{opt}V}{R} \tag{49}$$

where λ_{opt} is the optimum value of tip speed ratio of the wind turbine.

The desired value of the current i_{qs} can be calculated from the electromagnetic torque given in (16), such that:

$$x_{2d} = i^*_{qs} = \frac{2}{3}\frac{L_r}{pL_m}\frac{T_{mr}}{x_{3d}} \tag{50}$$

Note that T_{mr} is the input reference mechanical torque, and it is set to the maximum mechanical (aerodynamic) torque such that $T_{mr} = \frac{P_{m_{max}}}{x_{4d}}$.

The desired values of the direct and quadrature line currents i_{dg} and i_{qg} can be found from Equations (17), (34) and (35) after setting $P_g = P_s$ to transfer all active power from the side of the stator to the grid side while maintaining $Q_g = 0$ to ensure the unity power factor. Hence:

$$x_{5d} = i_{dg}^* = \frac{2}{3}\frac{P_s}{V_{grid}} \tag{51}$$

and the desired value of the quadrature line current i_{qg} is such that:

$$x_{6d} = i_{qg}^* = 0 \tag{52}$$

The DC-link voltage U_{dc} must be maintained constant at a preset value. The desired value of the voltage of the DC-link U_{dc} is such that:

$$U_{dc}^* = U_N \tag{53}$$

where U_N is the rated DC-bus voltage.

On the other hand, the input reference voltages v_{ds_r} and v_{qs_r} are computed using Equations (22) and (23) such that:

$$v_{ds_r} = \frac{1}{c_4}(c_1 x_{1d} - \omega_s x_{2d} - c_2 x_{3d}) \tag{54}$$

$$v_{qs_r} = \frac{1}{c_4}(c_1 x_{2d} + \omega_s x_{1d} + c_3 x_{3d} x_{4d} + \frac{2}{3}\frac{L_r}{pL_m}\frac{\dot{T}_{mr}}{x_{3d}}) \tag{55}$$

4. Control of the Wind Energy Power System

In this section, we will use the sliding mode control technique to control the wind energy conversion system. Figure 4 depicts the block diagram representation of the controlled SCIG-based WEC system.

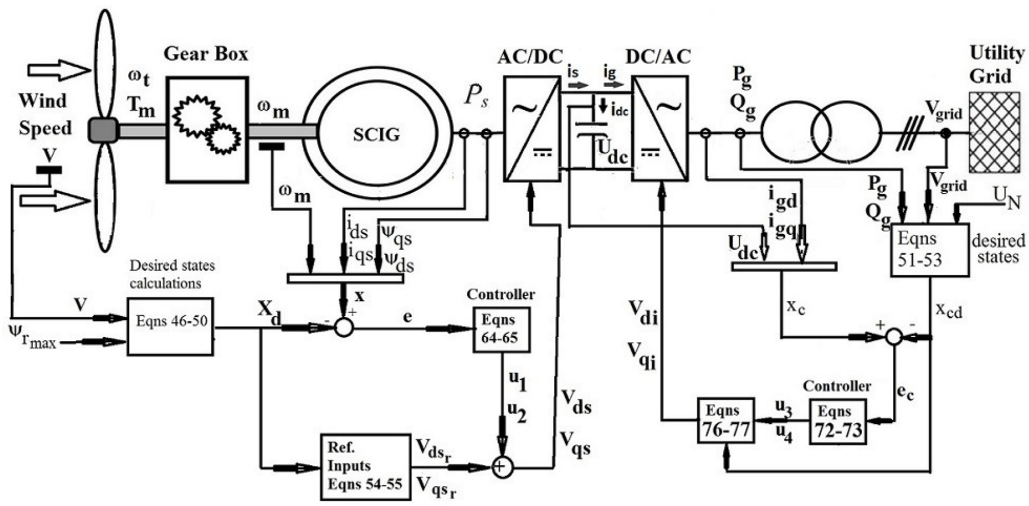

Figure 4. A block diagram representation of the controlled SCIG-based WEC.

4.1. Design of a Sliding Mode Controller for the Turbine and the Induction Generator

To facilitate the design of a controller for the wind turbine and induction generator system, we define the following nonlinear transformation:

$$\begin{aligned} z_1 &= e_3 \\ z_2 &= c_5 e_1 - c_6 e_3 \\ z_3 &= e_4 \\ z_4 &= c_7(e_2 e_3 + x_{3d} e_2 + x_{2d} e_3) - c_8 e_4 - c_9(T_m - T_{mr}) \end{aligned} \tag{56}$$

Using the above transformation, the dynamic model of wind turbine and induction generator error system in (27) can be written as follows:

$$\begin{aligned} \dot{z}_1 &= z_2 \\ \dot{z}_2 &= f_1 + g_1 u_1 \\ \dot{z}_3 &= z_4 \\ \dot{z}_4 &= f_2 + g_2 u_2 \end{aligned} \tag{57}$$

where f_1, f_2, g_1 and g_2 are such that:

$$f_1 = c_5\big(-c_1 e_1 + \omega_s e_2 + c_2 e_3\big) - c_6\big(c_5 e_1 - c_6 e_3\big) \tag{58}$$

$$\begin{aligned} f_2 = {} & c_7(e_3 + x_{3d})\big(-c_1 e_2 - \omega_s e_1 - c_3(e_3 e_4 + x_{4d} e_3 + x_{3d} e_4)\big) \\ & + c_7(e_2 + x_{2d})\big(c_5 e_1 - c_6 e_3\big) + c_7 e_2 \dot{x}_{3d} + c_7 e_3 \dot{x}_{2d} - c_9(\dot{T}_m - \dot{T}_{mr}) \\ & - c_8\big(c_7(e_2 e_3 + x_{3d} e_2 + x_{2d} e_3) - c_8 e_4 - c_9(T_m - T_{mr})\big) \end{aligned} \tag{59}$$

$$g_1 = c_4 c_5 \tag{60}$$

$$g_2 = c_4 c_7(e_3 + x_{3d}). \tag{61}$$

Let the design constants β_1, β_2, K_1, K_2, W_1 and W_2 be positive scalars. Define the sliding surfaces s_1 and s_2 such that:

$$s_1 = z_2 + \beta_1 z_1 \tag{62}$$

$$s_2 = z_4 + \beta_2 z_3 \tag{63}$$

Proposition 1. *The following sliding mode control law:*

$$u_1 = \frac{1}{g_1}\big(-f_1 - \beta_1 z_2 - K_1 s_1 - W_1 sign(s_1)\big) \tag{64}$$

$$u_2 = \frac{1}{g_2}\big(-f_2 - \beta_2 z_4 - K_2 s_2 - W_2 sign(s_2)\big) \tag{65}$$

when applied to the error system given by (27) guarantees that the errors e_i $(i = 1, ..., 4)$ converge to zero as t tends to infinity. Therefore, the states of the wind turbine and the induction generator given by (21) converge to their desired values as t tends to infinity.

Proof. Taking the time derivatives of s_1 and s_2 in (62) and (63), and using the dynamic model of the errors in (27) and the control laws given by (64) and (65), we obtain:

$$\begin{aligned} \dot{s}_1 &= \dot{z}_2 + \beta_1 \dot{z}_1 = f_1 + g_1 u_1 + \beta_1 z_2 \\ &= -K_1 s_1 - W_1 sign(s_1) \end{aligned} \tag{66}$$

and:

$$\begin{aligned} -K_2 s_2 - W_2 sign(s_2) &= \dot{z}_4 + \beta_2 \dot{z}_3 = f_2 + g_2 u_2 + \beta_2 z_4 \\ &= -K_2 s_2 - W_2 sign(s_2) \end{aligned} \quad (67)$$

From (66) and (67), we conclude that $\dot{s}_i = -K_i s_i - W_i sign(s_i)$ for $i = 1, 2$. It is clear that $s_i \dot{s}_i = -K_i s_i^2 - W_i |s_i|$ for $i = 1, 2$. Hence, the equations given by (66) and (67) guarantee that $s_i \dot{s}_i < 0$ when $s_i \neq$ for $i = 1, 2$. Therefore, the trajectories of these discontinuous dynamic equations exhibit a finite time reachability to zero from any given initial conditions provided that the gains K_1, K_2, W_1 and W_2 are chosen to be sufficiently large, strictly positive scalars.

Since s_1 and s_2 are driven to zero in finite time, then after such a finite time, we have $z_2 + \beta_1 z_1 = 0$ and $z_4 + \beta_2 z_3 = 0$. Thus, $z_2 = -\beta_1 z_1$ and $z_4 = -\beta_2 z_3$. Using the equations in (57), we can write: $\dot{z}_1 = z_2 = -\beta_1 z_1$, and $\dot{z}_3 = z_4 = -\beta_2 z_3$. The solutions of these two o.d.e.'s are, $z_1(t) = exp(-\beta_1 t) z_1(0)$ and $z_3(t) = exp(-\beta_2 t) z_3(0)$. Because β_1 and β_2 are positive scalars, it can be concluded that the states $z_1(t)$ and $z_3(t)$ tend to zero as t goes to infinity. Furthermore, since $s_1 = 0$ and $s_2 = 0$ on the sliding surfaces, it can be concluded that the variables $z_2(t)$ and $z_4(t)$ are driven to zero as t tends to infinity.

Using the transformation given by (56), it can be deduced that the errors $e_1(t)$, $e_2(t)$, $e_3(t)$ and $e_4(t)$ asymptotically converge to zero as t tends to infinity. □

Hence, it can be concluded that the application of the controller (64) and (65) to the model of the wind turbine and the induction generator system (21) guarantees the convergence of the states i_{ds}, i_{qs}, ψ_{dr} and ω_m to their desired values.

Remark 2. *The control laws v_{ds} and v_{qs}, which will be used to control the model of the wind turbine and the induction generator given by (21), are as follows:*

$$v_{ds} = u_1 + v_{ds_r} \quad (68)$$

$$v_{qs} = u_2 + v_{qs_r} \quad (69)$$

where v_{ds_r} and v_{qs_r} are obtained from (54) and (55).

4.2. Design of a Sliding Mode controller for the Grid Side Converter

This subsection deals with the design of a sliding mode controller for the grid side converter.

Let β_3, K_3, K_4, W_3 and W_4 be positive scalars. Furthermore, let B_d be a positive scalar bounding the "disturbance" d_p defined in (45) such that $|\dot{d}_p + \beta_3 d_p| \leq B_d$.

Define the sliding surfaces s_3 and s_4 such that:

$$s_3 = e_6 \quad (70)$$

$$s_4 = \dot{e}_7 + \beta_3 e_7 \quad (71)$$

Proposition 2. *The following sliding mode control law:*

$$u_3 = \frac{-1}{c_{12} v_{dg}} \left[c_{12} v_{dg} (-c_{10} e_5 + \omega e_6) + c_{12} \dot{v}_{dg} e_5 + c_{12} \beta_3 v_{dg} e_5 - K_4 s_4 - (B_d + W_4) sign(s_4) \right] \quad (72)$$

$$u_4 = c_{10} e_6 + \omega e_5 - K_3 s_3 - W_3 sign(s_3) \quad (73)$$

when applied to the model of the errors of the grid side converter given by (43) guarantees that the errors e_5, e_6 and e_7 converge to zero as t tends to infinity. Therefore, the states of the grid side converter converge to their desired values as t tends to infinity.

Proof. Let the Lyapunov function candidate V_x be such that:

$$V_x = \frac{1}{2}s_3^2 + \frac{1}{2}s_4^2 \tag{74}$$

Taking the derivative of V_x with respect to time along the trajectories of (43) and using the control law given by (72) and (73), we obtain:

$$\begin{aligned}
\dot{V}_x &= s_3\dot{s}_3 + s_4\dot{s}_4 = s_3\dot{e}_6 + s_4(\ddot{e}_7 + \beta_3\dot{e}_7) \\
&= s_3\big(- c_{10}e_6 - \omega e_5 + u_4\big) \\
&\quad + s_4\big(- c_{12}v_{dg}(-c_{10}e_5 + \omega e_6 + u_3) - c_{12}e_5\dot{v}_{dg} + \dot{d}_p + \beta_3(-c_{12}e_5v_{dg} + d_p)\big) \\
&= -K_3s_3^2 - W_3s_3sign(s_3) \\
&\quad + s_4\big(- c_{12}v_{dg}(-c_{10}e_5 + \omega e_6 + u_3) - c_{12}e_5\dot{v}_{dg} + \dot{d}_p + \beta_3(-c_{12}e_5v_{dg} + d_p)\big) \\
&\leq -K_3s_3^2 - W_3s_3sign(s_3) \\
&\quad + s_4\big(- c_{12}v_{dg}(-c_{10}e_5 + \omega e_6 + u_3) - c_{12}e_5\dot{v}_{dg} - \beta_3c_{12}e_5v_{dg}\big) + |s_4|B_d \\
&= -K_3s_3^2 - W_3s_3sign(s_3) \\
&\quad + s_4\big(- c_{12}v_{dg}(-c_{10}e_5 + \omega e_6 + u_3) - c_{12}e_5\dot{v}_{dg} - c_{12}\beta_3e_5v_{dg} + B_dsign(s_4)\big) \\
&= -K_3s_3^2 - W_3s_3sign(s_3) - K_4s_4^2 - W_4s_4sign(s_4) \\
&= -K_3s_3^2 - W_3|s_3| - K_4s_4^2 - W_4|s_4|
\end{aligned} \tag{75}$$

Therefore, $\dot{V}_x$ is negative definite. Hence, it can be concluded that the sliding surfaces s_3 and s_4 exhibit a finite time reachability to zero from any given initial conditions provided that the gains K_3, K_4, W_3 and W_4 are chosen to be sufficiently large, strictly positive scalars. Therefore, the error $e_6(t) = s_3(t)$ converges to zero in finite time. Furthermore, because β_3 is a positive scalar, we can conclude that the error $e_7(t)$ converge to zero as t tends to infinity.

Moreover, since s_3 and s_4 are driven to zero in finite time, then the controller u_3 after such time is: $u_3 = c_{10}e_5 - \frac{\dot{v}_{dg}}{v_{dg}}e_5 - \beta_3e_5$. Hence, after such time, the dynamics of the error e_5 is such that $\dot{e}_5 = -c_{10}e_5 + u_3 = -(\frac{\dot{v}_{dg}}{v_{dg}} + \beta_3)e_5$. Therefore, the error $e_5(t)$ asymptotically converges to zero provided that the control gain β_3 is chosen to be sufficiently large, strictly positive scalar. □

Hence, it can be concluded that the application of the controller (72) and (73) to the model of the grid side converter (41) guarantees the convergence of the states i_{dg}, i_{qg} and U_{dc} to their desired values.

Remark 3. *The control laws v_{d_i} and v_{q_i}, which will be used to control the model of the grid side converter given by (41), are as follows:*

$$v_{d_i} = \frac{1}{c_{11}}\big(u_3 + c_{10}x_{5d} - \omega x_{6d} + \dot{x}_{5d}\big) + v_{dg} \tag{76}$$

$$v_{q_i} = \frac{1}{c_{11}}\big(u_4 + c_{10}x_{6d} + \omega x_{5d} + \dot{x}_{6d}\big). \tag{77}$$

5. Simulation Results of the Proposed Sliding Mode Control Scheme

The performance of the SCIG-based wind energy conversion system given by (21) and (41) using the sliding mode controllers (68), (69), (76) and (77) was simulated using the MATLAB software. The parameters of the system used for the simulation studies are given in Table 1.

The model of the wind speed used for simulation purposes is given by the following formula [33],

$$\begin{aligned}
V &= 10 + 0.55[\sin(0.0625w) - 0.875\sin(0.1875w) + 0.75\sin(0.3125w) \\
&- 0.625\sin(0.625w) + 0.5\sin(1.875w) + 0.25\sin(3.125w) + 0.125\sin(6.25w)]
\end{aligned} \tag{78}$$

with $w = \frac{2\pi}{10}t$. The profile of the wind speed versus time is depicted in Figure 5.

Table 1. The parameters of the SCIG and the wind turbine.

Parameter	Value
The rated power	300 KW
The rated apparent power	300 KVA
The rated voltage (line to line)	575 v
The frequency/angular speed	$2\pi 50$ rad/s
The nominal frequency of the system	50 Hz
The resistance of the stator	0.0063 Ω
The leakage inductance of the stator	11.8 mH
The resistance of the rotor	0.0048 Ω
The leakage inductance of the rotor	11.6 mH
The magnetizing inductance	11.6 mH
The capacitor of the DC bus	20 mF
The rated voltage of the DC bus	760 v
The grid resistance	0.1 Ω
The grid leakage inductance	0.6 mH
The inertia of the generator	10.0 kg m^2
The number of pole pairs	2
The rated generator speed	158.7 rad/s
The rotor diameter of the wind turbine	14 m
The density of air	1.22 kg/m^3
The rated wind speed	12 m/s
The rated rotor speed	19.7 rpm
The gearbox ratio	23
The inertia of the turbine	50.0 kg m^2

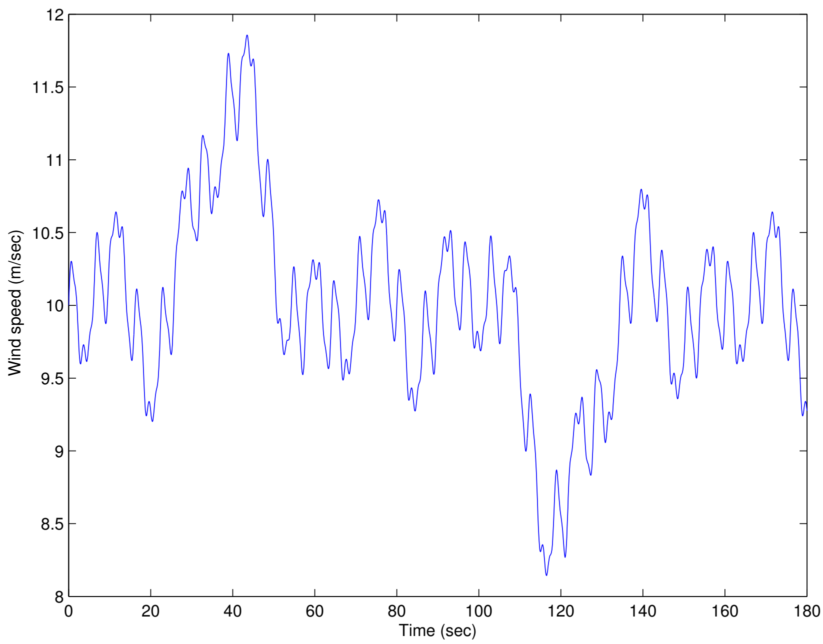

Figure 5. The profile of the wind speed versus time.

The simulation results are presented in Figures 6–17. The currents i_{ds} and i^*_{ds} versus time and the currents i_{qs} and i^*_{qs} versus time are depicted in Figures 6 and 7, respectively. It can be seen that the direct and quadrature currents are tracking their desired values. The fluxes ψ_{dr} and ψ^*_{dr} versus time are depicted in Figure 8. Figure 9 shows the angular speeds ω_m and ω^*_m of the generator versus time. It can be noticed that ω_m is tracking the desired speed and following the maximum power coefficient

$C_{p_{max}} = 0.47$, as shown in Figure 10. The electromagnetic torque T_{em} versus time and the stator active power P_s versus time are shown in Figures 11 and 12. For the grid side, the direct currents i_{dg} and i^*_{dg} versus time and the quadrature currents i_{qg} and i^*_{qg} versus time are presented in Figures 13 and 14, respectively. It is clear from these figures that the direct and quadrature currents track their desired values. The voltages U_{dc} and U^*_{dc} versus time are depicted in Figure 15. It is clear that the DC link voltage is almost constant at all times. Finally, the output active power of the grid P_g versus time and the output reactive power of the grid Q_g versus time are shown in Figures 16 and 17, respectively. Figure 16 shows that approximately all active power from the stator side has been transferred to the grid side. Furthermore, Figure 17 shows that the output reactive power of the grid Q_g is approximately zero, which ensures that the power factor is approximately one.

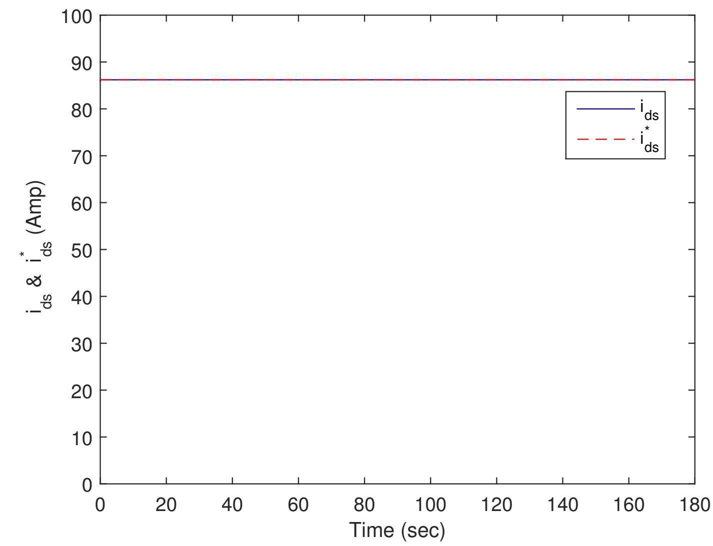

Figure 6. The currents i_{ds} and i^*_{ds} versus time.

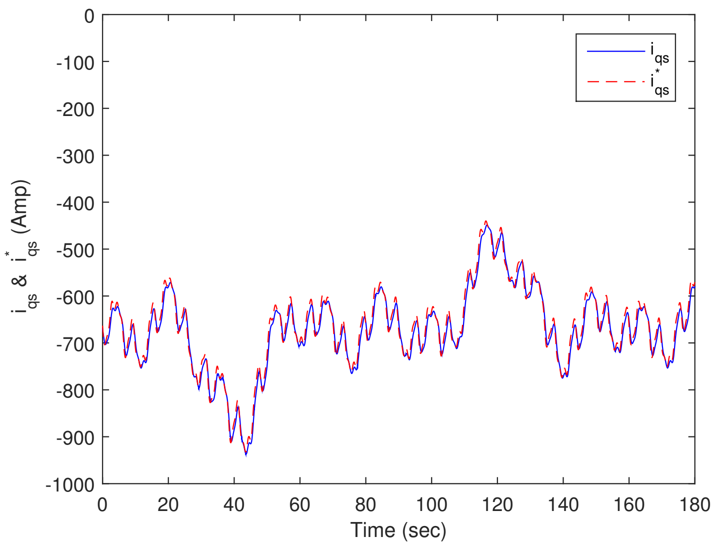

Figure 7. The currents i_{qs} and i^*_{qs} versus time.

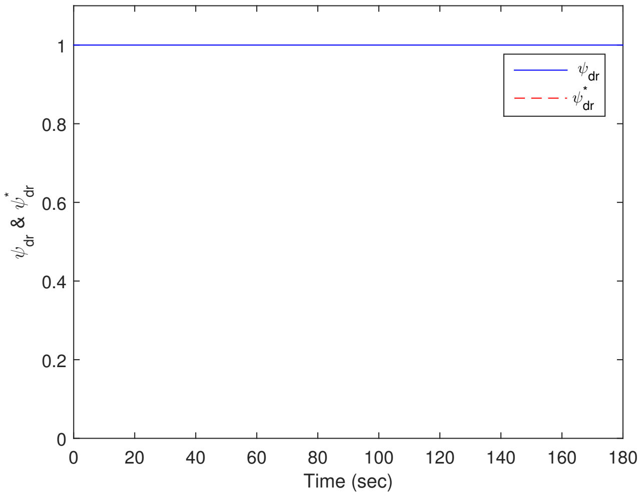

Figure 8. The fluxes ψ_{dr} and ψ^{*}_{dr} versus time.

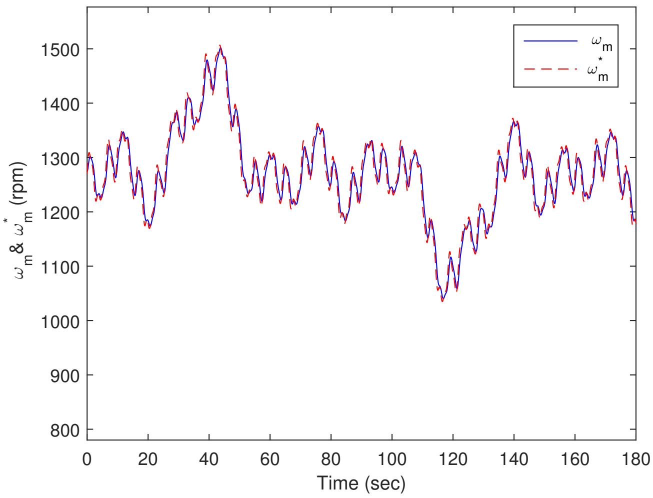

Figure 9. The angular speeds ω_m and ω^{*}_m versus time.

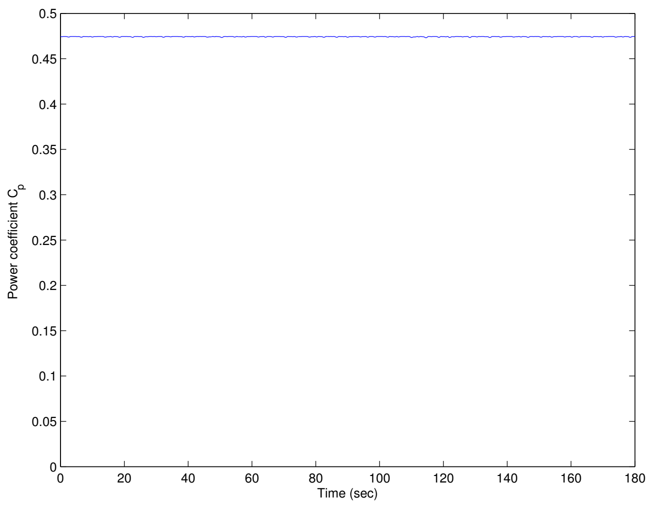

Figure 10. The power coefficient C_p versus time.

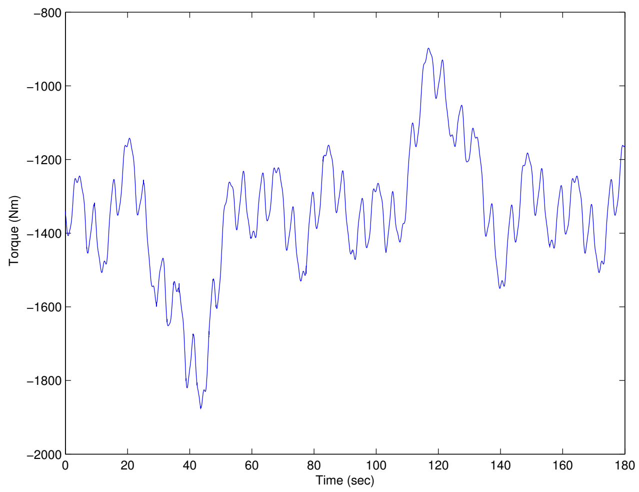

Figure 11. The electromagnetic torque T_{em} versus time.

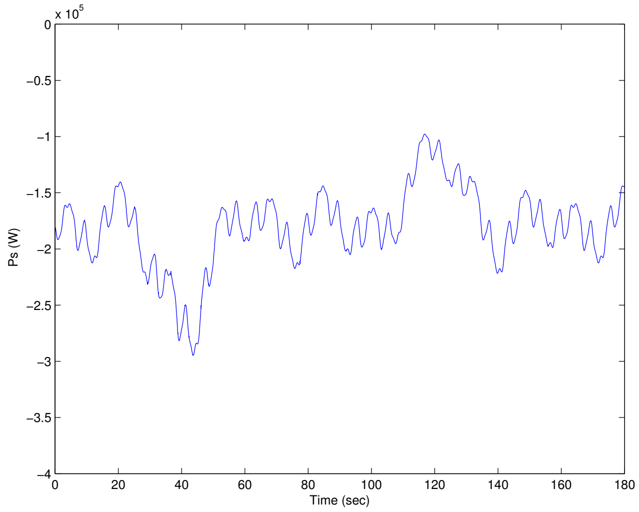

Figure 12. The active power of the stator P_s versus time.

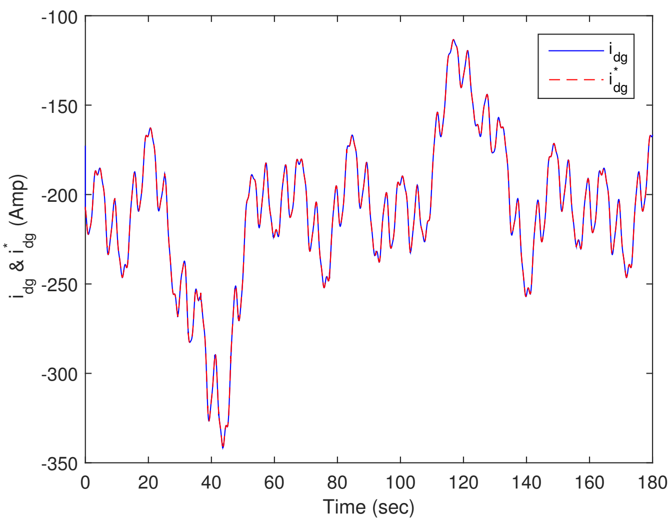

Figure 13. The currents i_{dg} and i^*_{dg} versus time.

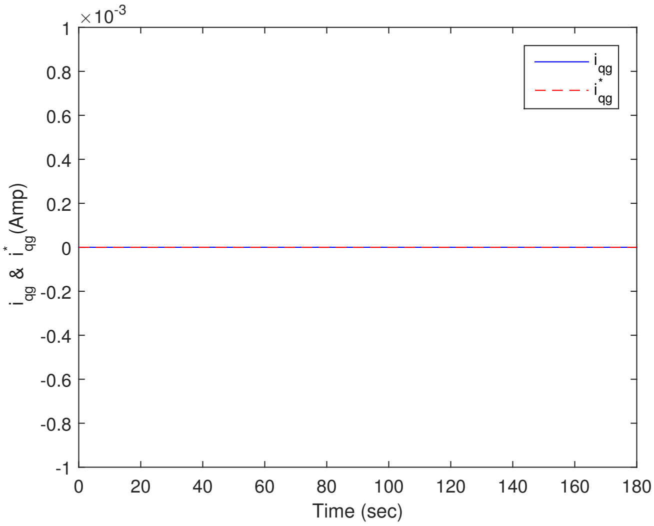

Figure 14. The currents i_{qg} and i_{qg}^{*} versus time.

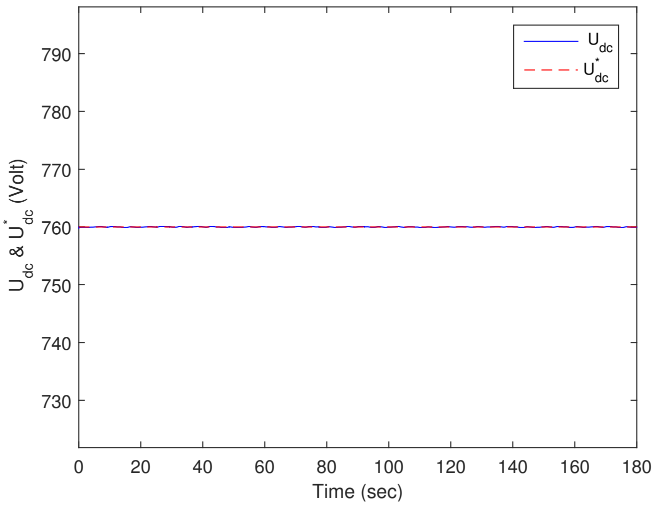

Figure 15. The voltages U_{dc} and U_{dc}^{*} versus time.

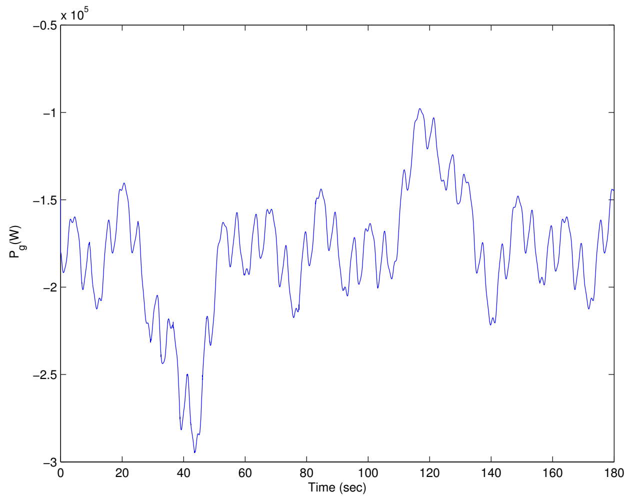

Figure 16. The output active power of the grid P_g versus time (negative sign for produced power).

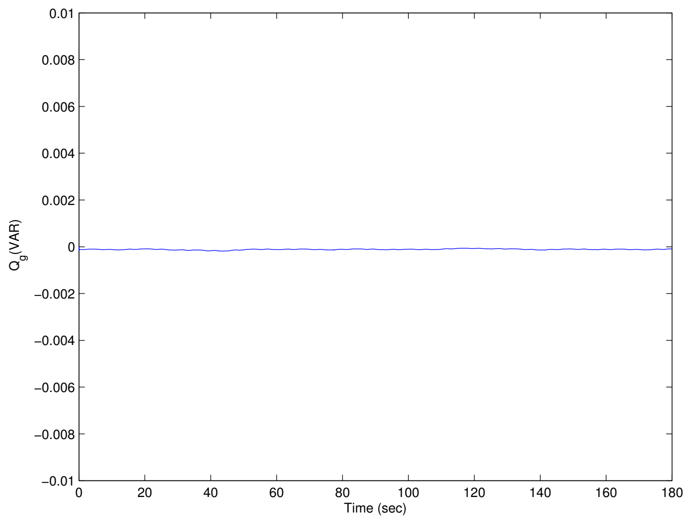

Figure 17. The output reactive power of the grid Q_g versus time.

The simulation results clearly indicate that the proposed sliding mode control scheme when applied to the a squirrel cage induction generator-based wind energy conversion system is able to force the states of the system to converge to their desired values. Hence, the controller enables maximum extraction of power from the wind at different speeds of the wind, and it ensures that the generated active power is transmitted through the DC-bus to the grid while maintaining the unity power factor.

6. Conclusions

This paper dealt with the control of a squirrel cage induction generator-based wind energy conversion system. Sliding mode controllers are proposed for the WEC system so that the actual states of the system track the desired states of the system. The control laws are designed to control the stator side converter, as well as the grid side converter. The stability of the controlled system is analyzed. Furthermore, simulation results are presented to verify the validity of the proposed control scheme. The simulation results indicate that the proposed sliding mode control scheme works well.

Future work will address the design of observer-based controllers for SCIG-based wind energy conversion systems.

Author Contributions: Mohamed Zribi and Muthana Alrifai contributed equally to this work. Mohamed Rayan contributed to the simulations of the performance of the system. The final manuscript was approved by all authors.

Conflicts of Interest: The authors declare no conflict of interest.

References

1. Baloch, M.H.; Wang, J.; Kaloi, G.S. A Review of the State of the Art Control Techniques for Wind Energy Conversion System. *Int. J. Renew. Energy Res. (IJRER)* **2016**, *6*, 1276–1295.
2. Li, H.; Chen, Z. Overview of Different wind generator systems and their comparisons. *IET Renew. Power Gener.* **2008**, *2*, 123–138.
3. Mahela, O.P.; Shaik, A.G. Comprehensive overview of grid interfaced wind energy generation systems. *Renew. Sustain. Energy Rev.* **2016**, *57*, 260–281.
4. Cheng, M.; Zhu, Y. The state of the art of wind energy conversion systems and technologies: A review. *Energy Convers. Manag.* **2014**, *88*, 332–347.
5. Chen, Z.; Guerrero, J.M.; Blaabjerg, F. A review of the state of the art of power electronics for wind turbines. *IEEE Trans. Power Electron.* **2009**, *24*, 1859–1875.
6. Nguyen, H.M.; Naidu, D.S. Evolution of wind turbine control systems. In *Encyclopedia of Control Systems, Robotics, and Automation*; EOLSS Publishers: Oxford, UK, 2010.
7. Pao, L.Y.; Johnson, K.E. Control of wind turbines. *IEEE Control Syst.* **2011**, *31*, 44–62.

8. Babu, N.R.; Arulmozhivarman, P. Wind energy conversion systems-a technical review. *J. Eng. Sci. Technol.* **2013**, *8*, 493–507.
9. Benchagra, M.; Errami, Y.; Hilal, M.; Maaroufi, M.; Cherkaoui, M.; Ouassaid, M. New control strategy for inductin generator-wind turbine connected grid. In Proceedings of the 2012 International Conference on Multimedia Computing and Systems (ICMCS), Tangiers, Morocco, 10–12 May 2012; pp. 1043–1048.
10. Benchagra, M.; Hilal, M.; Errami, Y.; Ouassaid, M.; Maaroufi, M. Modeling and control of SCIG based variable-speed with power factor control. *Int. Rev. Model. Simul. (IREMOS)* **2011**, *4*, 1007–1014.
11. Benchagra, M.; Maaroufi, M.; Ouassaid, M. A performance comparison of linear and nonlinear control o f a SCIG-wind farm connecting to a distribution network. *Turk. J. Electr. Eng. Comput. Sci.* **2014**, *22*, 1–11.
12. Benchagra, M.; Maaroufi, M. Control of wind farm connected distribution network. In Proceedings of the 10th IEEE International Conference on Networking, Sensing and Control (ICNSC), Evry, France, 10–12 April 2013; pp. 467–472.
13. Benchagra, M.; Maaroufi, M.; Ouassaid, M. Nonlinear MPPT control of squirrel cage induction generator-wind turbine. *J. Theor. Appl. Inf. Technol.* **2012**, *35*, 26–33.
14. Wang, P.; Wang, H.; Cai, X.; Han, Z. Passivity-based robust controller design for a variable speed wind energy conversion system. *Turk. J. Electr. Eng. Comput. Sci.* **2016**, *24*, 558–570.
15. Hassan, A. Nonlinear Control of Variable wind Speed Conversion System Based on a Squirrel Cage Induction Generator (SCIG). *Am. J. Eng. Appl. Sci.* **2015**, *8*, 275–284.
16. Zhao, H.; Wu, Q.; Rasmussen, C.N.; Blanke, M. $calL_1$ Adaptive Speed Control of a Small Wind Energy Conversion System for Maximum Power Point Tracking. *IEEE Trans. Energy Convers.* **2014**, *29*, 576–584.
17. Heydari-doostabad, H.; Khalghani, M.R.; Khooban, M.H. A novel control system design to improve LVRT capability of fixed speed wind turbines using STATCOM in presence of voltage fault. *Int. J. Electr. Power Energy Syst.* **2016**, *77*, 280–286.
18. Baloch, M.H.; Wang, J.; Kaloi, G.S. Stability and nonlinear controller analysis of wind energy conversion system with random wind speed. *Int. J. Electr. Power Energy Syst.* **2016**, *79*, 75–83.
19. Domínguez-García, J.L.; Gomis-Bellmunt, O.; Trilla-Romero, L.; Junyent-Ferré, A. Indirect vector control of a squirrel cage induction generator wind turbine. *Comput. Math. Appl.* **2012**, *64*, 102–114.
20. Ouassaid, M.; Elyaalaoui, K.; Cherkaoui, M. Sliding Mode Control of Induction Generator Wind Turbine Connected to the Grid. In *Advances and Applications in Nonlinear Control Systems*; Springer International Publishing: New York, NY, USA, 2016; pp. 531–553.
21. Amimeur, H.; Aouzellag, D.; Abdessemed, R.; Ghedamsi, K. Sliding mode control of a dual-stator induction generator for wind energy conversion systems. *Int. J. Electr. Power Energy Syst.* **2012**, *42*, 60–70.
22. De Battista, H.; Mantz, R.J.; Christiansen, C.F. Dynamical sliding mode power control of wind driven induction generators. *IEEE Trans. Energy Convers.* **2010**, *15*, 451–457.
23. Mi, Y.; Bao, X.; Yang, Y.; Zhang, H.; Wang, P. The sliding mode pitch angle controller design for squirrel-cage induction generator wind power generation system. In Proceedings of the 33rd Chinese Control Conference (CCC), Nanjing, China, 28–30 July 2014; pp. 8113–8117.
24. Beltran, B.; Ahmed-Ali, T.; Benbouzid, M.E. High-order sliding-mode control of variable-speed wind turbines. *IEEE Trans. Ind. Electron.* **2009**, *56*, 3314–3321.
25. Leon, A.E.; Farias, M.F.; Battaiotto, P.E.; Solsona, J.A.; Valla, M.I. Control strategy of a DVR to improve stability in wind farms using squirrel-cage induction generators. *IEEE Trans. Power Syst.* **2011**, *26*, 1609–1617.
26. Senjyu, T.; Ochi, Y.; Muhando, E.; Urasaki, N.; Sekine, H. Speed and position sensor-less maximum power point tracking control for wind generation system with squirrel cage induction generator. In Proceedings of the 2006 IEEE PES Power Systems Conference and Exposition, Atlanta, GA, USA, 29 October–1 November 2006; pp. 2038–2043.
27. Senjyu, T.; Ochi, Y.; Kikunaga, Y.; Tokudome, M.; Yona, A.; Muhando, E.B.; Urasaki, N.; Funabashi, T. Sensor-less maximum power point tracking control for wind generation system with squirrel cage induction generator. *Renew. Energy* **2009**, *34*, 994–999.
28. Faiz, J. Design and Implementation of a Solid-state Controller for Regulation of Output Voltage of a Wind-driven Self-excited three-phase Squirrel-cage Induction Generator. In Proceedings of the International Conference on Electrical Machines and Systems, Nanjing, China, 27–29 September 2005.
29. Duong, M.Q.; Grimaccia, F.; Leva, S.; Mussetta, M.; Ogliari, E. Pitch angle control using hybrid controller for all operating regions of SCIG wind turbine system. *Renew. Energy* **2014**, *70*, 197–203.

30. Duong, M.Q.; Grimaccia, F.; Leva, S.; Mussetta, M.; Le, K.H. Improving transient stability in a grid-connected squirrel-cage induction generator wind turbine system using a fuzzy logic controller. *Energies* **2015**, *8*, 6328–6349.
31. Xu, P.; Shi, K.; Bu, F.; Zhao, D.; Fang, Z.; Liu, R.; Zhu, Y. A Vertical-Axis Off-Grid Squirrel-Cage Induction Generator Wind Power System. *Energies* **2016**, *9*, 822.
32. Pena, R.; Clare, J.C.; Asher, G.M. Doubly fed induction generator using back-to-back PWM converters and its application to variable-speed wind-energy generation. *IEE Proc.-Electr. Power Appl.* **1996**, *143*, 231–241.
33. Alrifai, M.; Zribi, M.; Rayan, M. Feedback Linearization Controller for a Wind Energy Power System. *Energies* **2016**, *9*, 771.